BuGZ exhibits guanine nucleotide exchange activity toward tubulin

Wesley J. Yon[1,2,7], Joseph R. Tran[1], Taekjip Ha[3,4,5,6], Yixian Zheng[1], and Ross T.A. Pedersen[1]

[1] Department of Embryology, Carnegie Institution for Science, Baltimore, MD, USA
[2] Department of Biology, Johns Hopkins University, Baltimore, MD, USA
[3] Department of Biophysics, Johns Hopkins University, Baltimore, MD, USA
[4] Department of Biophysics and Biophysical Chemistry, Johns Hopkins University School of Medicine, Baltimore, MD, USA
[5] Department of Biomedical Engineering, Johns Hopkins University School of Medicine, Baltimore, MD, USA
[6] Howard Hughes Medical Institute, Baltimore, MD, USA
[7] Corresponding author: wyon@carnegiescience.edu

Abstract

α- and β-tubulin, which form heterodimers that assemble into microtubules, are GTPases. Like other GTPases, the nucleotide-bound state of tubulin heterodimers controls whether the molecules are in a biologically active or inactive state. While α-tubulin in the heterodimer is constitutively bound to GTP, β-tubulin can be bound to either GDP (GDP-tubulin) or GTP (GTP-tubulin). GTP-tubulin hydrolyzes its GTP to GDP following assembly into a microtubule and, upon disassembly, must exchange its bound GDP for GTP to participate in subsequent microtubule polymerization. Tubulin dimers have been shown to exhibit rapid intrinsic nucleotide exchange *in vitro,* leading to a commonly accepted belief that a tubulin guanine nucleotide exchange factor (GEF) may be unnecessary in cells. Here, we use quantitative binding assays to show that BuGZ, a spindle assembly factor, binds tightly to GDP-tubulin, less tightly to GTP-tubulin, and weakly to microtubules. We further show that BuGZ promotes the incorporation of GTP into tubulin using a nucleotide exchange assay. The discovery of a tubulin GEF suggests a mechanism that may aid rapid microtubule assembly dynamics in cells.

Introduction

Microtubules (MT) are a component of the eukaryotic cytoskeleton required for key cellular functions including transportation of cargo via motor proteins, relaying of mechanical signals to the interphase nucleus, and proper segregation of chromosomes during cell division (1–5). Microtubules are composed of tubulin, a small GTPase. Tubulin is a heterodimer of α- and β-tubulin in which α-tubulin is constitutively bound to guanosine triphosphate (GTP), while β-tubulin's nucleotide is exchangeable, with the identity of the bound nucleotide dictating the assembly competence of the heterodimer (6). Tubulin heterodimers with GTP-bound β-tubulin (hereinafter referred to as GTP-tubulin) can incorporate into growing microtubule ends. As the microtubule elongates, β-tubulin hydrolyzes its GTP, forming GDP-tubulin in the microtubule lattice. GDP-tubulin in the microtubule lattice assumes a curved conformation that disfavors microtubule growth and promotes catastrophe, causing a switch from growth to shrinkage (7–9). Following microtubule disassembly, free GDP-tubulin is then released into the cytosol and must exchange its GDP for GTP before it can take part in microtubule polymerization again.

Similarly to microtubules, actin filaments, another component of the cytoskeleton, are assembled from nucleotide-bound subunits that hydrolyze their nucleotide. Free, ATP-bound, actin monomers are incorporated into actin filaments, where, like microtubule subunits, they eventually hydrolyze their bound nucleotide (10). Disassembly of actin filaments produces free ADP-actin, which must exchange its bound ADP for ATP to regain assembly competence. Uncatalyzed dissociation of nucleotide from actin is slow ($t_{1/2}$ = 69 s), but is accelerated 75-fold by profilin, facilitating binding of a new nucleotide, with ATP binding favored by the 15:1 ratio of ATP:ADP in the cell. (11, 12). In contrast with actin, GDP-tubulin quickly unbinds GDP *in vitro* ($t_{1/2}$ = 5 s) and binds to free GTP or GDP. Since the GTP:GDP ratio in cells is ~10:1, tubulin is generally thought to readily exchange bound GDP for GTP to replenish the pool of assembly-competent subunits even without a nucleotide exchange factor (13).

Unlike tubulin, many GTPases intrinsically exchange nucleotides on timescales too slow for proper biological function and require guanine nucleotide exchange factors (GEF) to exchange their nucleotides on biologically relevant timescales (14–18). GEFs contain GTPase family-specific catalytic domains (CDC25 homology domains for RasGEFs, Sec7 domain for ArfGEFs, etc.), and do not share structural characteristics across different families. However, studies have shown that GEFs bind GTPases and mediate the release of nucleotides by displacing the magnesium ion required for stable nucleotide binding. GEFs bind to GTPases irrespective of their nucleotide states and mediate the exchange of either GTP or GDP with nucleotides in solution (19, 20). *In vivo*, the high ratio of cytosolic GTP:GDP results in an equilibrium where the presence of a GEF ensures that most GTPases are bound to GTP. Tubulin's intrinsically high rate of nucleotide exchange may explain the lack of known tubulin GEFs despite the discovery of myriad interacting proteins for microtubules and tubulin. Given that nearly all physiological chemical reactions are catalyzed by enzymes, a tubulin GEF may be necessary in cellular states with rapid microtubule assembly and disassembly (21–23).

BuGZ (Bub3-interacting and GLEBS motif-containing protein ZNF207) is a tubulin and microtubule-binding protein and has been shown to regulate spindle assembly and promote proper microtubule-kinetochore attachment in mitosis. Loss of BuGZ results in prometaphase arrest with defects in spindle morphology and chromosome alignment (24–26). BuGZ is an evolutionarily conserved spindle assembly factor identified in animals and plants (27). Furthermore, BuGZ directly binds to microtubules/tubulin through its N-terminal 92 amino acid domain containing two C2H2 zinc fingers. BuGZ undergoes liquid-liquid phase separation through its intrinsically disordered regions, such that BuGZ coacervates concentrate soluble tubulin dimers and promote microtubule polymerization activity (26). Here, we report the results of a systematic series of quantitative binding assays demonstrating that BuGZ binds most strongly to GDP-tubulin. We further present evidence that BuGZ promotes nucleotide exchange on tubulin, converting GDP-tubulin back to GTP-tubulin. We will discuss the functional implication of our findings on microtubule assembly dynamics in cellular contexts.

Results

BuGZ exhibits weak binding to microtubules

Previous studies have shown that BuGZ binds to microtubules and tubulin dimers to promote microtubule polymerization and bundling (24, 26). However, quantification of BuGZ's ability to bind microtubules has not been reported. Therefore, we performed quantitative binding assays to determine the binding affinity between BuGZ and microtubules.

To measure equilibrium binding of BuGZ to microtubules, we used microtubules polymerized with a 1:10 mixture of biotinylated:unlabeled GTP-tubulin such that ≥1 biotin-tubulin is present per 12-protofilament turn, facilitating retrieval of the microtubules with paramagnetic streptavidin beads. (28). Given that taxol-stabilized microtubules are stable over a wide temperature range, we performed all equilibrium binding experiments at 4˚C to suppress BuGZ's tendency to undergo liquid-liquid phase separation which generates confounding oligomeric structures (26, 29). To measure binding affinity, we mixed 1.19 μM *Xenopus laevis* BuGZ and varying concentrations of taxol-stabilized microtubules (0 μM, 5.5 μM, 11 μM, 22 μM, 44 μM, 110 μM), allowed time for the reaction to reach equilibrium, then retrieved the microtubule-bound streptavidin beads magnetically. The supernatant was collected and BuGZ depletion was measured by quantitative Western blot analysis. Plots of the BuGZ fraction bound vs. microtubule concentration were fit to rectangular hyperbolas (see Materials and Methods) and the K_D was determined from the fit. We measured BuGZ's equilibrium dissociation constant (K_D) for taxol-stabilized microtubules to be 9.57 μM (95% CI: 7.35 μM - 12.35 μM)(Figure 1A). A similar fraction of BuGZ bound to 10 μM unperturbed microtubules and to 10 μM sheared microtubules, suggesting that BuGZ binds along the wall of microtubules and does not show obvious preference to microtubule ends under our assay conditions (Figure 1A, 1B).

BuGZ preferentially binds GDP-tubulin over GTP-tubulin

The above findings show that BuGZ's affinity for intact microtubules was relatively weak. Since BuGZ is also known to concentrate free tubulin dimers into phase-separated droplets, we wondered how well BuGZ binds free tubulin dimers (26). We first investigated BuGZ's binding affinity for GTP-tubulin. Varying concentrations (0 μM, 0.1 μM, 1 μM, 2 μM, 5 μM, 10 μM, 20 μM) of biotinylated GTP-tubulin were bound to streptavidin-coated paramagnetic beads and mixed with 1.19 μM BuGZ. The beads were retrieved via magnetic separation, and BuGZ binding was assessed by measuring BuGZ depletion from the supernatant via quantitative Western blot analysis. From the hyperbolic fit, BuGZ's K_D for GTP-tubulin was determined to be 477 nM (95% CI: 193.4 nM - 948.9 nM) (Figure 2A).

The 20X difference between BuGZ's K_D for GTP-tubulin compared to taxol-microtubules prompted us to further measure the binding affinity of BuGZ to GDP-tubulin using the same assay. BuGZ's K_D for GDP-tubulin was 45.3 nM (95% CI: 33.6 nM - 59.0 nM): 10X higher affinity than for GTP-tubulin and 210X higher affinity than for taxol-microtubules (Figure 2B). BuGZ's stronger affinities for tubulin dimers over microtubules, regardless of nucleotide state, led us to conclude that BuGZ is a tubulin associated protein.

BuGZ promotes GTP exchange into GDP-tubulin

BuGZ's preferential binding of GDP-tubulin over GTP-tubulin led us to investigate why a protein would bind preferentially to GDP-tubulin, an assembly-deficient state of tubulin. We hypothesized that BuGZ might promote nucleotide exchange to convert GDP-tubulin into GTP-tubulin. To test this hypothesis, we compared the incorporation of GTP α-^{32}P into GDP-tubulin in the presence and absence of BuGZ. 1 mM GTP including 3 nM GTP α-^{32}P was added to a solution of 100 μM GDP-tubulin and 1 mM GDP to achieve a 1:1 ratio of GTP:GDP,. Then, BuGZ or BSA were added to a final concentration of 1.19μM. We hypothesized that if BuGZ preferentially promotes nucleotide exchange on GDP-tubulin because of its stronger binding affinity, the presence of BuGZ would result in higher GTP incorporation into tubulin, even in the presence of a 1:1 ratio of available GTP and GDP. At equilibrium, nucleotides were cross-linked to tubulin via UV radiation and unbound nucleotides were removed using a desalting column. Radiolabeling of the tubulin and BuGZ eluted from the desalting column was assessed by a scintillation counter (Figure 3A). In the presence of BuGZ, GTP incorporation, measured by the exchange of GDP for ^{32}P-labeled GTP, increased by 60% (p=0.016) (Figure 3B).

Discussion

Our quantitative binding assays show that BuGZ binds tubulin dimers with >20-fold stronger affinity than to microtubules. Previous studies have shown that BuGZ promotes microtubule polymerization *in vitro* and proposed a model in which BuGZ coacervation concentrates tubulin dimers such that the local concentration of dimers in the droplet microenvironment are sufficient

to drive microtubule polymerization (26). Subsequent studies of phase-separating microtubule regulators, such as Tau and centrosome components, have advanced a similar model (30–32). Our results in this study may appear contradictory with previous results showing BuGZ interactions with microtubules *in vitro*. However, *in vitro* stabilization of microtubules with taxol often involves processing steps in which unincorporated dimers are washed out of the system such that microtubules are the only ligand available for BuGZ to bind. In light of our findings, we would expect BuGZ to bind primarily to soluble tubulin dimers rather than to microtubules in a system in which both tubulin dimers and microtubules are present (*e.g. in vivo*).

We found that BuGZ binds GDP-tubulin with a 10-fold stronger affinity than it binds GTP-tubulin. The tubulin affinity of other tubulin binding proteins (e.g., XMAP215, Tau, CLASP) has primarily been studied for free GTP-tubulin. CLIP-170 is an exception, as it has been shown to have higher affinity for GTP- and GDP-tubulin than for assembled microtubules, but unlike BuGZ, CLIP-170 binds slightly more strongly to GTP-tubulin than to GDP-tubulin (33). The exclusion of soluble GDP-tubulin when studying protein-tubulin interactions was reasonable in light of the generally accepted view that GDP-tubulin is rapidly exchanged into GTP-tubulin such that no mediating factor is required. However, myriad studies have shown nucleotide- and assembly-state dependent structural differences of tubulin, and many microtubule associated proteins recognize these conformational differences and decorate specific regions of assembled microtubules that are rich in either GTP-tubulin (near the growing end) or GDP-tubulin (far from the growing end) (7, 8, 34, 35). Therefore, it is plausible that many previously characterized tubulin-binding proteins might also exhibit nucleotide-specific binding to free tubulin that has previously been unappreciated.

We have shown, using a radio-nucleotide exchange assay, that BuGZ promotes GTP incorporation into soluble tubulin dimers. We favor a model in which BuGZ binding to tubulin primes the dimer for nucleotide exchange. In this model, BuGZ's higher affinity for GDP-tubulin than for GTP-tubulin, paired with the high GTP:GDP ratio of in cells would result in BuGZ preferentially promoting dissociation of GDP in exchange for GTP. In situations of high microtubule dynamicity, such as during mitotic spindle assembly, BuGZ's GEF activity may be critical for maintaining GTP-tubulin levels for proper spindle assembly, as seen by previous work demonstrating spindle defects in BuGZ-depleted cells (24, 25, 36). Higher microtubule dynamicity results in higher concentrations of GDP-tubulin from depolymerization, which may make necessary a GEF to replenish the GTP-tubulin pool to support continued microtubule polymerization activity. This proposed mechanism is consistent with BuGZ's subcellular localization in interphase vs. mitosis. In interphase cells, the majority of BuGZ is nuclear, isolated from tubulin and microtubules in the cytoplasm (24, 25). Upon entry into mitosis, BuGZ protein levels increase, the nuclear envelope breaks down, and BuGZ is enriched on the mitotic spindle, where it may engage in this proposed GEF reaction (36). Further studies will need to investigate both the physiological importance of BuGZ's *in vitro* GEF activity and potential tubulin GEFs among known microtubule associated proteins.

Materials and Methods

Cloning, protein expression, protein purification

Xenopus laevis BuGZ cDNA, codon-optimized for *Spodoptera frugiperda* Sf9 expression, was cloned into a baculovirus vector (Gibco pFastBac Dual Expression Vector) via Gibson Assembly (NEB Gibson Assembly Master Mix). In the assembled plasmid, BuGZ (NCBI: NM_001086855.1) is tagged on its amino terminus with: four leader amino acids, then a 6x His tag, then a GS linker, and finally a modified TEV protease cleavage site (full tag sequence: MSYY-HHHHHH-GSG$_4$SG$_4$S-ENLYFQG). Vectors were then transfected into Sf9 cells (Gibco Sf9 cells in Sf-900 SFM), using Gibco Cellfectin II Reagent according to ThermoFisher Bac-to-Bac Baculovirus Expression System instructions, to generate P0 viral stock. After 3 rounds of viral amplification, corresponding P3 virus was used to infect Sf9 cells for protein expression. 72 hrs post-infection, cells were collected into 100 mL pellets via centrifugation at 1,000 x g. Pellets were snap-frozen in liquid nitrogen and stored at -80˚C. For purification, pellets were thawed and resuspended in lysis buffer (LyB): 20 mM KH_2PO_4, 500 mM NaCl, 25 mM Imidazole, 1 mM $MgCl_2$, 1 mM β-mercaptoethanol, 2.5% Glycerol, 0.01% Triton X-100, Roche cOmplete, EDTA-free Protease Inhibitor Cocktail, pH 7.4. The cell suspension was sonicated using Misonix Sonicator 3000 (2 min. total process time, 30 s on, 30 s off, power level 2.0) on ice and then clarified by centrifugation at 15,000 x g for 30 min. Clarified lysate was then filtered through MilliporeSigma Millex-GP 0.22 µm PES membrane filter unit. Lysate was loaded onto a 1 mL HisTrap HP column (Cytiva) equilibrated in Buffer A (same as LyB without protease inhibitor cocktail). The column was then washed with 1X lysate volume of 85% Buffer A/15% Buffer B (20 mM KH_2PO_4, 150 mM NaCl, 300 mM Imidazole, 1 mM $MgCl_2$, 1 mM β-mercaptoethanol, 2.5% Glycerol, 0.01% Triton X-100, pH 7.4). Bound protein was eluted with a 30 mL linear gradient from 15% to 100% Buffer B. BuGZ-containing fractions were identified by running samples on SDS polyacrylamide gels and stained with Invitrogen SimplyBlue SafeStain. BuGZ-positive fractions were pooled and concentrated to <500 µL using Millipore Amicon Ultra centrifugation units with 30 kDa MW cut off. Contaminating proteins were removed from the concentrated BuGZ protein solution by gel filtration using a Superdex 200 Increase 10/300 GL column equilibrated in Buffer C (80 mM PIPES pH6.8, 100 mM KCl, 1 mM $MgCl_2$, 50 mM Sucrose, 1 mM EGTA). Fractions of the eluate containing BuGZ were again identified on SDS polyacrylamide gels and were then pooled, and concentrated using Millipore Amicon Ultra centrifugation units, and snap-frozen in liquid nitrogen for storage at -80˚C. The purity and concentration of BuGZ was determined by comparing in-gel SimplyBlue SafeStain staining to staining of known amounts of bovine serum albumin.

Measurement of BuGZ binding to Taxol-stabilized microtubules

10 mg/mL tubulin (Cytoskeleton T240) and 1 mg/mL biotin-tubulin (Cytoskeleton T333P) were mixed in equal volumes in a buffer containing BRB80 (80mM PIPES, 1mM $MgCl_2$, 1mM EGTA, pH 6.8) + 1 mM GTP. The tubulin solution was diluted 1:1 in a solution containing BRB80, 2 mM

DTT, 2 mM GTP, 20 μM taxol (taxol buffer 1) and incubated for 20 min. at 37˚C. Pierce Streptavidin Magnetic Beads (ThermoFisher Scientific 88816) were equilibrated in a buffer containing BRB80, 1 mM DTT, 1 mM GTP, 10 μM taxol (taxol buffer 2). The binding reaction mixture was added to 20μL streptavidin-coated beads and incubated for 20 min. at 4˚C, then washed 3 times with taxol buffer 2. After the final wash, the beads were resuspended in a 10μL solution containing taxol buffer 2 and 1.19 μM BuGZ. After 20 min. incubation at 4˚C, the beads were collected with a magnet and the supernatant was removed, and mixed with an equal volume of 2X SDS sample buffer for immunoblot analysis. For experiments with sheared microtubules, the taxol-stabilized microtubules were passed through a 30 G syringe needle 10 times immediately prior to addition to streptavidin-coated beads.

Measurement of BuGZ binding to GTP- and GDP-Tubulin

Varying volumes of solution containing 1 mg/mL (~10 μM) biotin-tubulin, 200 μM nocodazole, 1 mM GTP or GDP, and BRB80 were added to Pierce Streptavidin Magnetic Beads equilibrated in the same buffer to decorate them with the desired amount of tubulin. After 20 min. incubation at 4˚C, beads were washed 3 times in the same buffer and supernatant was removed. The magnetic beads, now decorated with varying amounts of biotin tubulin, were resuspended in equal volumes of a solution containing 1.19 μM BuGZ, 200 μM nocodazole, 1 mM GTP or GDP, and BRB80. After 15 min. incubation at 4˚C, beads were pelleted and supernatant was collected (mixed 50% v/v with 2X Laemmli buffer) for immunoblot analysis.

Gel electrophoresis and immunoblot blot analysis

Supernatants from binding experiments were boiled at 95˚C for 10 min. and spun down in a benchtop centrifuge at 10,000 g for 3 min. Samples were loaded into an SDS polyacrylamide gel and separated by electrophoresis in a Tris-Glycine buffer (25 mM Tris, 250 mM glycine, 3.5 mM SDS). Following electrophoresis, proteins were transferred onto nitrocellulose membrane (Cytiva Amersham 10600002) for 2 hrs at 4˚C in transfer buffer (50 mM Tris, 125 mM glycine, 3.5 mM SDS, 20% methanol). After transfer, membranes were incubated in a block buffer (5% w/v skim milk, Tris-buffered saline) for 1 hr at room temperature, then probed with primary antibodies to the 6X His tag (for BuGZ recognition) in 5% w/v skim milk, Tris-buffered saline, 0.02% Tween-20, for 1 hr at room temperature. After washing 3 times for 10 min. each in tris-buffered saline, membranes were incubated in a secondary antibody solution (Tris-buffered saline, 0.02% Tween-20, antibody) for 1 hr at room temperature. After washing 3 times for 10 min. in tris-buffered saline, membranes were imaged in a LI-COR CLx system. Anti-6X His tag antibody (ab18184) was diluted at 1:1000, and the secondary antibody, LI-COR IRDye 680RD Goat anti-Mouse IgG, was diluted at 1:10,000.

Nucleotide exchange assay

A solution containing 100 μM tubulin, 1 mM GDP, BRB80 was mixed with a 1/10 volume of 10X nucleotide exchange buffer (10 mM GTP, 30 nM GTP α-^{32}P (PerkinElmer BLU506H250UC), 1 mM nocodazole, BRB80) for a final solution containing 91 μM tubulin, 0.9 μM GDP, 0.9 μM GTP, 2.7 nM GTP α-^{32}P, 91 μM nocodazole, and BRB80. Immediately, a BRB80 solution containing either BuGZ or BSA was added to a final concentration of 1.19 μM of the protein. Corresponding controls were produced in the same manner except without the addition of tubulin. Mixtures

were incubated at room temperature for 15 min. Then, samples were treated with UV for 5 min. in a Stratagene UV Stratalinker 1800. Free nucleotides were removed with BioRad Micro Bio-Spin 6 gel columns (BioRad 7326222) equilibrated to BRB80 buffer according to manufacturer's instructions. Flowthrough was mixed with a scintillation cocktail (RPI Bio-Safe II) and GTP α-^{32}P was measured using PerkinElmer Tri-Carb 2810 TR. The measured signal from the no tubulin conditions for BSA or BuGZ were subtracted from its corresponding tubulin + BuGZ or BSA readouts. Then, the data were normalized as a ratio of the BuGZ to BSA ^{32}P signals

Statistical analysis

All statistical analyses were performed using Graphpad Prism 9. Sheared vs. unsheared microtubule binding (Fig 1B) statistics performed using parametric unpaired t-tests. Equilibrium dissociation constants were determined using the function:

$$Y = \frac{K_d + X + B - \sqrt{(K_d + X + B)^2 - 4XB}}{2B}$$

where X is the microtubule/tubulin concentration, and B is the concentration of BuGZ.

Acknowledgments

The authors would like to thank Ashish Tiwary (Carnegie Institution for Science) for helpful discussion. The study was funded by NIH NIGMS GM106023 (awarded to Yixian Zheng and Robert Goldman), NIH NIGMS GM110151 (awarded to Yixian Zheng), NIH NIGMS F32 GM142145 (awarded to Ross T.A. Pedersen), and NIH NIGMS R35 GM122569 (awarded to Taekjip Ha).

1. Gudimchuk, N. B., and McIntosh, J. R. (2021) Regulation of microtubule dynamics, mechanics and function through the growing tip. *Nat Rev Mol Cell Bio*. **22**, 777–795
2. Sleigh, J. N., Rossor, A. M., Fellows, A. D., Tosolini, A. P., and Schiavo, G. (20**19**) Axonal transport and neurological disease. *Nat Rev Neurol*. **15**, 691–703
3. Reck-Peterson, S. L., Redwine, W. B., Vale, R. D., and Carter, A. P. (2018) The cytoplasmic dynein transport machinery and its many cargoes. Nat Rev Mol Cell Bio. 19, 382–398
4. Zheng, Y. (2010) A membranous spindle matrix orchestrates cell division. *Nat Rev Mol Cell Biology*. **11**, 529–35
5. Kirby, T. J., and Lammerding, J. (2018) Emerging views of the nucleus as a cellular mechanosensor. *Nat Cell Biol*. **20**, 373–381
6. Mandelkow, E., and Mandelkow, E.-M. (1994) Microtubule structure. *Curr Opin Struc Biol*. **4**, 171–179
7. Alushin, G. M., Lander, G. C., Kellogg, E. H., Zhang, R., Baker, D., and Nogales, E. (2014) High-Resolution Microtubule Structures Reveal the Structural Transitions in αβ-Tubulin upon GTP Hydrolysis. Cell. **157**, 1117–1**129**
8. Knossow, M., Campanacci, V., Khodja, L. A., and Gigant, B. (2020) The Mechanism of Tubulin Assembly into Microtubules: Insights from Structural Studies. *Iscience*. **23**, 101511
9. Horio, T., and Murata, T. (2014) The role of dynamic instability in microtubule organization. *Front Plant Sci*. **5**, 511
10. Pollard, T. D., Blanchoin, L., and Mullins, R. D. (2000) MOLECULAR MECHANISMS CONTROLLING ACTIN FILAMENT DYNAMICS IN NONMUSCLE CELLS. *Annu Rev Bioph Biom*. **29**, 545–576
11. Goldschmidt-Clermont, P. J., Furman, M. I., Wachsstock, D., Safer, D., Nachmias, V. T., and Pollard, T. D. (1992) The control of actin nucleotide exchange by thymosin beta 4 and profilin. A potential regulatory mechanism for actin polymerization in cells. *Mol Biol Cell*. **3**, 1015–1024
12. Traut, T. W. (1994) Physiological concentrations of purines and pyrimidines. *Mol Cell Biochem*. **140**, 1–22
13. Brylawski, B. P., and Caplow, M. (1983) Rate for nucleotide release from tubulin. *J Biol Chem*. **258**, 760–763
14. Self, A. J., and Hall, A. (1995) Measurement of intrinsic nucleotide exchange and GTP hydrolysis rates. *Methods Enzymol*. **256**, 67–76
15. Kopra, K., Ligabue, A., Wang, Q., Syrjänpää, M., Blaževitš, O., Veltel, S., Adrichem, A. J. van, Hänninen, P., Abankwa, D., and Härmä, H. (2014) A homogeneous quenching resonance energy transfer assay for the kinetic analysis of the GTPase nucleotide exchange reaction. *Anal Bioanal Chem*. **406**, 4147–4156
16. Lim, C., Berk, J. M., Blaise, A., Bircher, J., Koleske, A. J., Hochstrasser, M., and Xiong, Y. (2020) Crystal structure of a guanine nucleotide exchange factor encoded by the scrub typhus pathogen Orientia tsutsugamushi. *Proc National Acad Sci*. **117**, 30380–30390
17. Marshall, C. B., Meiri, D., Smith, M. J., Mazhab-Jafari, M. T., Gasmi-Seabrook, G. M. C., Rottapel, R., Stambolic, V., and Ikura, M. (2012) Probing the GTPase cycle with real-time NMR: GAP and GEF activities in cell extracts. Methods. **57**, 473–485

18. Chardin, P., Camonis, J. H., Gale, N. W., Aelst, L. van, Schlessinger, J., Wigler, M. H., and Bar-Sagi, D. (1993) Human Sos1: a Guanine Nucleotide Exchange Factor for Ras that Binds to GRB2. *Science*. **260**, 1338–1343
19. Béraud-Dufour, S., Robineau, S., Chardin, P., Paris, S., Chabre, M., Cherfils, J., and Antonny, B. (1998) A glutamic finger in the guanine nucleotide exchange factor ARNO displaces Mg2+ and the β-phosphate to destabilize GDP on ARF1. *Embo J*. **17**, 3651–3659
20. Bos, J. L., Rehmann, H., and Wittinghofer, A. (2007) GEFs and GAPs: Critical Elements in the Control of Small G Proteins. Cell. 129, 865–877
21. Yu, N., Signorile, L., Basu, S., Ottema, S., Lebbink, J. H. G., Leslie, K., Smal, I., Dekkers, D., Demmers, J., and Galjart, N. (2016) Isolation of Functional Tubulin Dimers and of Tubulin-Associated Proteins from Mammalian Cells. *Curr Biol*. **26**, 1728–1736
22. Littauer, U. Z., Giveon, D., Thierauf, M., Ginzburg, I., and Ponstingl, H. (1986) Common and distinct tubulin binding sites for microtubule-associated proteins. Proc National Acad Sci. **83**, 7162–7166
23. Bodakuntla, S., Jijumon, A. S., Villablanca, C., Gonzalez-Billault, C., and Janke, C. (2019) Microtubule-Associated Proteins: Structuring the Cytoskeleton. *Trends Cell Biol*. **29**, 804–819
24. Jiang, H., He, X., Wang, S., Jia, J., Wan, Y., Wang, Y., Zeng, R., Yates, J., Zhu, X., and Zheng, Y. (2014) A microtubule-associated zinc finger protein, BuGZ, regulates mitotic chromosome alignment by ensuring Bub3 stability and kinetochore targeting. *Dev Cell*. **28**, 268–81
25. Toledo, C. M., Herman, J. A., Olsen, J. B., Ding, Y., Corrin, P., Girard, E. J., Olson, J. M., Emili, A., DeLuca, J. G., and Paddison, P. J. (2014) BuGZ Is Required for Bub3 Stability, Bub1 Kinetochore Function, and Chromosome Alignment. Dev Cell. 28, 282–94
26. Jiang, H., Wang, S., Huang, Y., He, X., Cui, H., Zhu, X., and Zheng, Y. (2015) Phase Transition of Spindle-Associated Protein Regulate Spindle Apparatus Assembly. Cell. **163**, **108**–122
27. Chin, A. F., Zheng, Y., and Hilser, V. J. (2022) Phylogenetic convergence of phase separation and mitotic function in the disordered protein BuGZ. *Protein Sci*. **31**, 822–834
28. Díaz, J. F., Valpuesta, J. M., Chacón, P., Diakun, G., and Andreu, J. M. (1998) Changes in Microtubule Protofilament Number Induced by Taxol Binding to an Easily Accessible Site INTERNAL MICROTUBULE DYNAMICS*. J Biol Chem. **273**, 33803–33810
29. SCHIFF, P. B., FANT, J., and HORWITZ, S. B. (1979) Promotion of microtubule assembly in vitro by taxol. *Nature*. **277**, 665–667
30. Hernández-Vega, A., Braun, M., Scharrel, L., Jahnel, M., Wegmann, S., Hyman, B. T., Alberti, S., Diez, S., and Hyman, A. A. (2017) Local Nucleation of Microtubule Bundles through Tubulin Concentration into a Condensed Tau Phase. *Cell Reports*. **20**, 2304–2312
31. Wiegand, T., and Hyman, A. A. (2020) Drops and fibers — how biomolecular condensates and cytoskeletal filaments influence each other. *Emerg Top Life Sci*. 10.1042/etls20190174
32. Woodruff, J. B., Gomes, B. F., Widlund, P. O., Mahamid, J., Honigmann, A., and Hyman, A. A. (2017) The Centrosome Is a Selective Condensate that Nucleates Microtubules by Concentrating Tubulin. Cell. **169**, 1066-1077.e10
33. Folker, E. S., Baker, B. M., and Goodson, H. V. (2005) Interactions between CLIP-170, Tubulin, and Microtubules: Implications for the Mechanism of CLIP-170 Plus-End Tracking Behavior. Mol Biol Cell. 16, 5373–5384

34. Maurer, S. P., Bieling, P., Cope, J., Hoenger, A., and Surrey, T. (2011) GTPγS microtubules mimic the growing microtubule end structure recognized by end-binding proteins (EBs). Proc National Acad Sci. 108, 3988–3993
35. Brouhard, G. J., Stear, J. H., Noetzel, T. L., Al-Bassam, J., Kinoshita, K., Harrison, S. C., Howard, J., and Hyman, A. A. (2008) XMAP215 Is a Processive Microtubule Polymerase. Cell. **132**, 79–88
36. Jiang, H., He, X., Feng, D., Zhu, X., and Zheng, Y. (2015) RanGTP aids anaphase entry through Ubr5-mediated protein turnover. *J Cell Biology*. **211**, 7–18

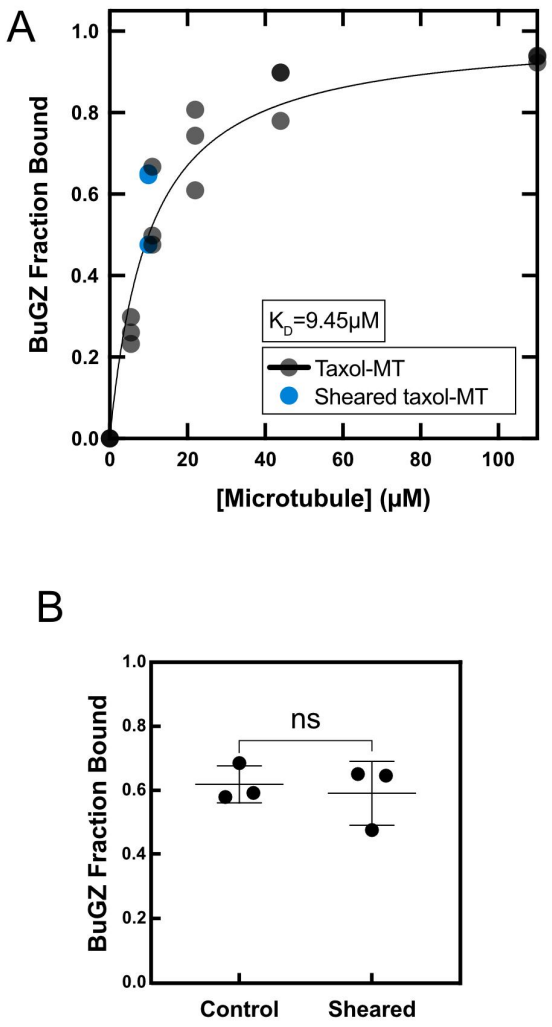

Figure 1 BuGZ exhibits weak binding to microtubules. (A) BuGZ binding isotherm to taxol-microtubules. K_D = 9.45 μM (95% CI = 7.16 μM - 12.3 μM). Three replicates for each measured concentration. Gray circles are for unsheared microtubules, while blue circles are for sheared microtubules (only one BuGZ concentration was used in the binding assay for sheared microtubules see B). The circles appear dark when they overlap. (B) BuGZ fraction bound to 10 μM unsheared and sheared taxol-microtubules.

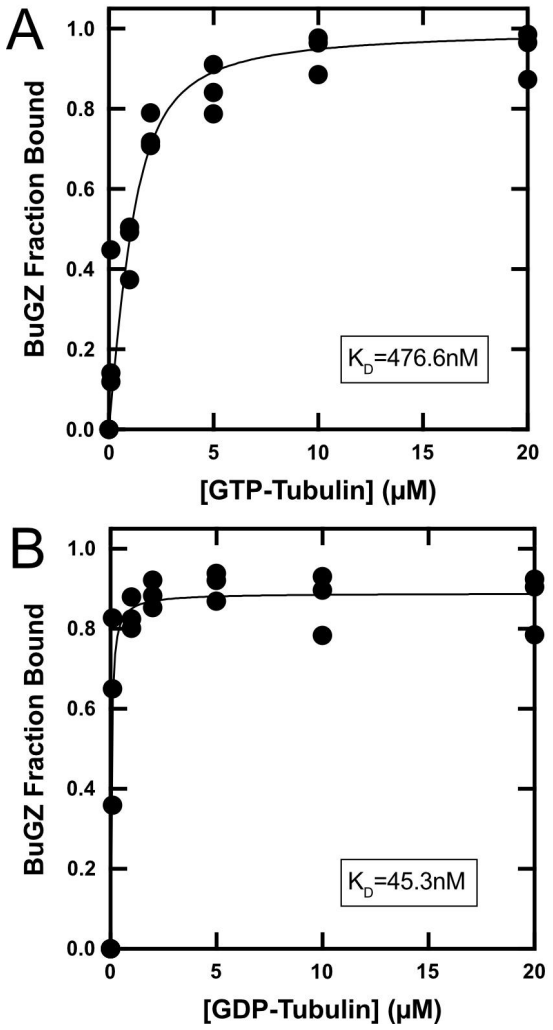

Figure 2 BuGZ exhibits preferential binding to GDP-tubulin over GPT-tubulin. (A) BuGZ binding isotherm to GTP-tubulin. K_D = 476.6 nM (95% CI = 193.4 nM - 949.0 nM). (B) BuGZ binding isotherm to GDP-tubulin. K_D = 45.3 nM (95% CI = 33.6 nM - 59.0 nM).

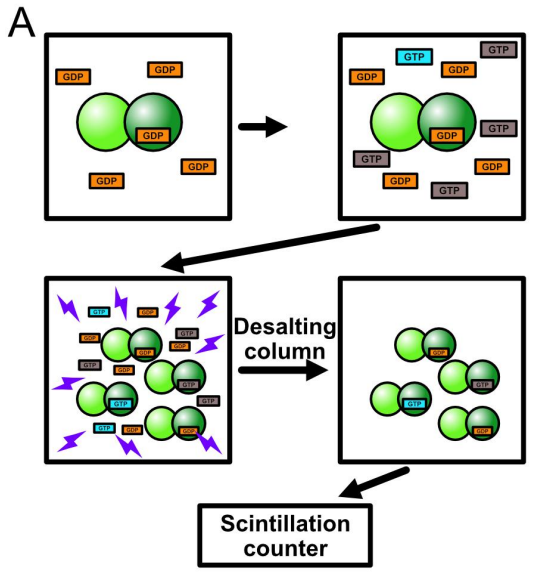

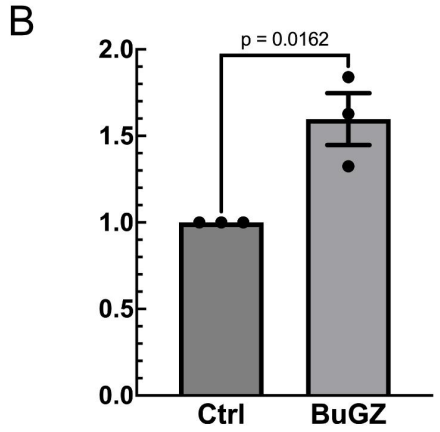

Figure 3 BuGZ acts as a guanine nucleotide exchange factor (GEF) on tubulin. (A) Workflow of BuGZ GEF assay. Tubulin dimers in 1mM GDP buffer are supplemented with nocodazole, BuGZ (or BSA control), equimolar GTP, and spike-in of ^{32}P-GTP. After 15 min. incubation, the mixture undergoes UV-crosslinking. Desalting column was used to remove unincorporated nucleotides and tubulin-associated radioactive GTP was measured with a scintillation counter. Light green = α-tubulin. Dark green = β-tubulin. Orange = GDP. Grey = GTP. Cyan = ^{32}P-GTP. (B) BuGZ promotes ^{32}P-GTP incorporation into tubulin by 60.0% relative to BSA control ($p = 0.0162$).